JOURNAL OF GEOPHYSICAL RESEARCH, VOL. 103, NO. A6, PAGES 11,685–11,694, JUNE 1, 1998

Global energy deposition during the January 1997 magnetic cloud event

G. Lu,[1] D. N. Baker,[2] R. L. McPherron,[3] C. J. Farrugia,[4] D. Lummerzheim,[5]
J. M. Ruohoniemi,[6] F. J. Rich,[7] D. S. Evans,[8] R. P. Lepping,[9]
M. Brittnacher,[10] X. Li,[2] R. Greenwald,[6] G. Sofko,[11] J. Villain,[12] M. Lester,[13]
J. Thayer,[14] T. Moretto,[15] D. Milling,[16] O. Troshichev,[17] A. Zaitzev,[18]
V. Odintzov,[18] G. Makarov,[19] and K. Hayashi[20]

Abstract. The passage of an interplanetary magnetic cloud at Earth on January 10–11, 1997, induced significant geomagnetic disturbances, with a maximum AE in excess of 2000 nT and a minimum Dst of about -85 nT. We use a comprehensive set of data collected from space-borne instruments and from ground-based facilities to estimate the energy deposition associated with the three major magnetospheric sinks during the event. It is found that averaged over the 2-day period, the total magnetospheric energy deposition rate is about 400 GW, with 190 GW going into Joule heating rate, 120 GW into ring current injection, and 90 GW into auroral precipitation. By comparison, the average solar wind electromagnetic energy transfer rate as represented by the ϵ parameter is estimated to be 460 GW, and the average available solar wind kinetic power U_{SW} is about 11,000 GW. A good linear correlation is found between the AE index and various ionospheric parameters such as the cross-polar-cap potential drop, hemisphere-integrated Joule heating rate, and hemisphere-integrated auroral precipitation. In the northern hemisphere where the data coverage is extensive, the proportionality factor is 0.06 kV/nT between the potential drop and AE, 0.25 GW/nT between Joule heating rate and AE, and 0.13 GW/nT between auroral precipitation and AE. However, different studies have resulted in different proportionality factors. One should therefore be cautious when using empirical formulas to estimate the ionospheric energy deposition. There is an evident saturation of the cross-polar-cap potential drop for large AE (>1000 nT), but further studies are needed to confirm this.

[1]High Altitude Observatory, NCAR, Boulder, Colorado.
[2]Laboratory for Atmospheric and Space Physics, University of Colorado, Boulder.
[3]Institute of Geophysics and Planetary Physics, University of California, Los Angeles.
[4]Space Science Center, University of New Hampshire, Durham.
[5]Geophysical Institute, University of Alaska, Fairbanks.
[6]Applied Physics Laboratory, Johns Hopkins University, Maryland.
[7]Phillips Laboratory, Hanscom Air Force Base, Massachusetts.
[8]Space Environment Center, NOAA, Boulder, Colorado.
[9]NASA Goddard Space Flight Center, Greenbelt, Maryland.
[10]Department of Geophysics, University of Washington, Seattle.
[11]Department of Physics and Engineering Physics, University of Saskatchewan, Saskatoon, Saskatchewan, Canada.
[12]Laboratoire de Physique et Chimie de l'Environnement, CNRS, Orleans, France.
[13]Department of Physics, University of Leicester, Leicester, England.
[14]SRI International, Menlo Park, California.
[15]Danish Meteorological Institute, Copenhagen, Denmark.
[16]Department of Physics, University of York, York, England.
[17]Geophysics Department, Arctic and Antarctic Research Institute, St. Petersburg, Russia.
[18]IZMIRAN, Troitsk, Russia.
[19]Institute of Cosmophysical Research and Aeronomy, Yakutsk, Russia.
[20]Department of Earth and Planetary Physics, University of Tokyo, Tokyo, Japan.

Paper number 98JA00897.
0148-0227/98/98JA-00897$09.00

1. Introduction

Through solar wind-magnetosphere interaction, a fraction of the incoming solar wind energy is deposited into the Earth's magnetosphere as auroral precipitation and Joule heating in the high-latitude ionosphere, as ring current energization in the inner magnetosphere,

as plasma sheet particle heating and plasmoid ejection in the magnetotail. During the periods of interplanetary disturbances such as magnetic clouds, energy input from the solar wind can have a dramatic impact on the near-Earth space environment [*Farrugia et al.*, 1997]. It is therefore important to understand quantitatively the different magnetospheric energy deposition processes.

In this paper we examine the energy deposition in the high-latitude ionosphere as well as in the ring current during the January 1997 magnetic cloud event. We use the assimilative mapping of ionospheric electrodynamics (AMIE) procedure to characterize the high-latitude ionospheric response to the magnetic cloud by combining the various observations from space- and ground-based instruments. The estimate of ring current energy injection rate is based on empirical formulas. We also compare the magnetospheric energy deposition with the available solar wind energy inputs. Uncertainties associated with the different energy estimates are discussed later in the paper. Results are compared with other previous investigations.

2. Observations and Results

2.1. Solar Wind and IMF Conditions

Figure 1 shows the 1-min averaged solar wind and interplanetary magnetic field measurements from the Wind satellite, which was located at about (85, -59, -4) R_E and (101, -55, -6) R_E in GSE (X, Y, Z) coordinates at 0000 UT on January 10 and 12, 1997, respectively. Figure 1 shows, from top to bottom, the solar wind bulk flow speed, the solar wind dynamic pressure (assuming exclusively a proton population), and the B_z component (the solid curve) as well as the magnitude of the IMF (the dotted curve). The magnetic cloud arrived at Wind at 0442 UT on January 10 (as marked by the vertical dashed line) and lasted for about 2200 hours as the interplanetary magnetic field gradually rotated from strongly southward to northward, while the total magnetic field strength remained nearly constant. The cloud was preceded by an interplanetary shock at ~0040 UT on January 10, as seen from the impulsive changes in all parameters shown in Figure 1. At the

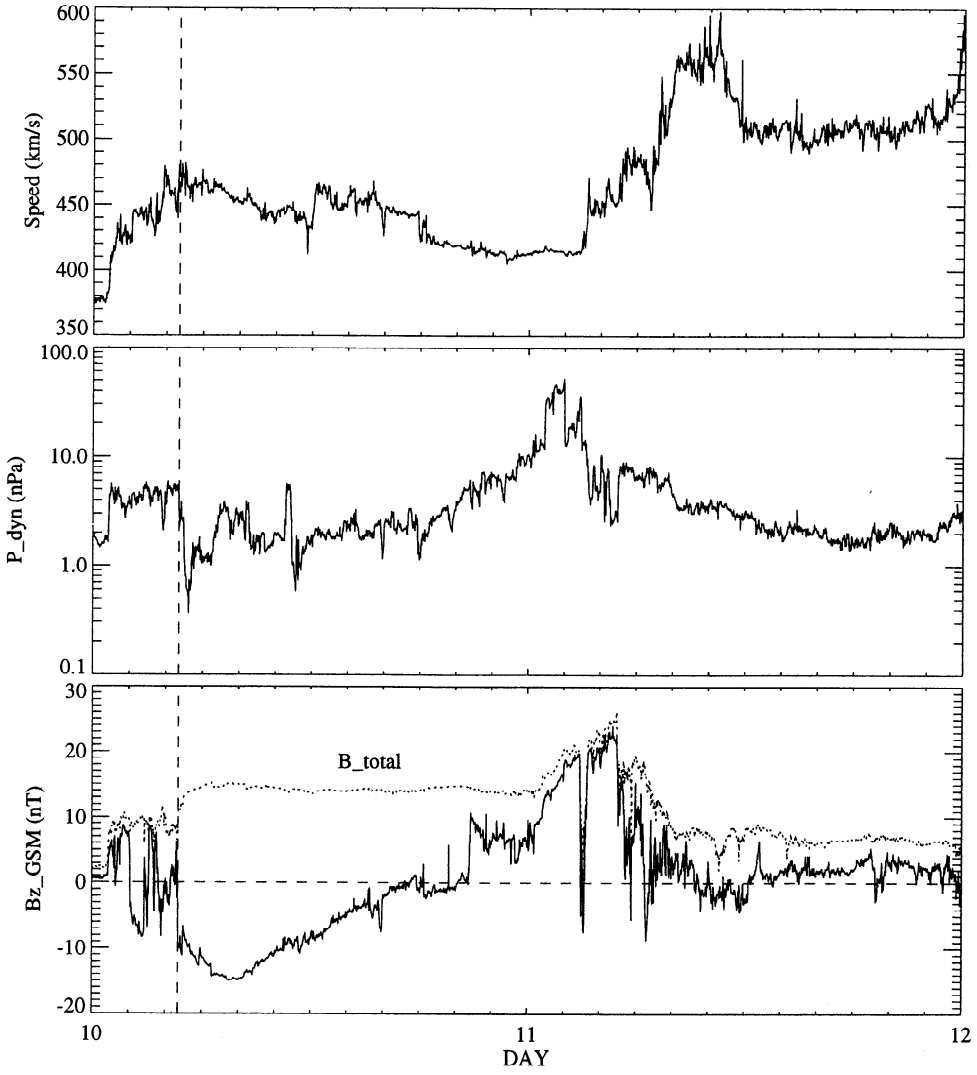

Figure 1. One-minute solar wind and interplanetary magnetic fields (in GSM coordinates) measured by the Wind satellite during the period of January 10–11, 1997.

rear of the cloud the solar wind dynamic pressure increased dramatically, which was caused by a burst of high-density plasma thought to be prominence material [*Burlaga et al.*, 1998]. The cloud was being overtaken by a faster corotating stream. The large variability of the solar wind plasma density (not shown) led to a dynamic pressure varying over a range of 2 orders of magnitude. This magnetic cloud event has been discussed in more detail by *Farrugia et al.* [1998] and *Burlaga et al.* [1998].

2.2. AMIE Procedure

AMIE is an optimally constrained, weighted, least squares fit of coefficients to global observations [*Richmond and Kamide*, 1988]. It first modifies the statistical conductivity and auroral energy flux models by incorporating direct and indirect observations of auroral precipitation and the height-integrated Pedersen and Hall conductances to provide an improved temporal and spatial resolution of these ionospheric quantities. In this study we have used statistical models of *Fuller-Rowell and Evans* [1986], which are parameterized by the 10 levels of hemispheric power index. In the second step, the procedure estimates the ionospheric convection pattern based on the direct ion drift observations from polar-orbiting satellites and radars and from the inversion of ground magnetic perturbations with the aid of ionospheric conductances. The different data sets are weighted according to their effective errors so that less reliable data contribute less to the fitting (see *Richmond and Kamide* [1988] for more information).

During the 2-day period (January 10–11, 1997) under study, there are various data sets available, including the ion drift and auroral precipitation measurements from the DMSP F10, F12, and F13 satellites, auroral precipitation observations from the NOAA 12 and 14

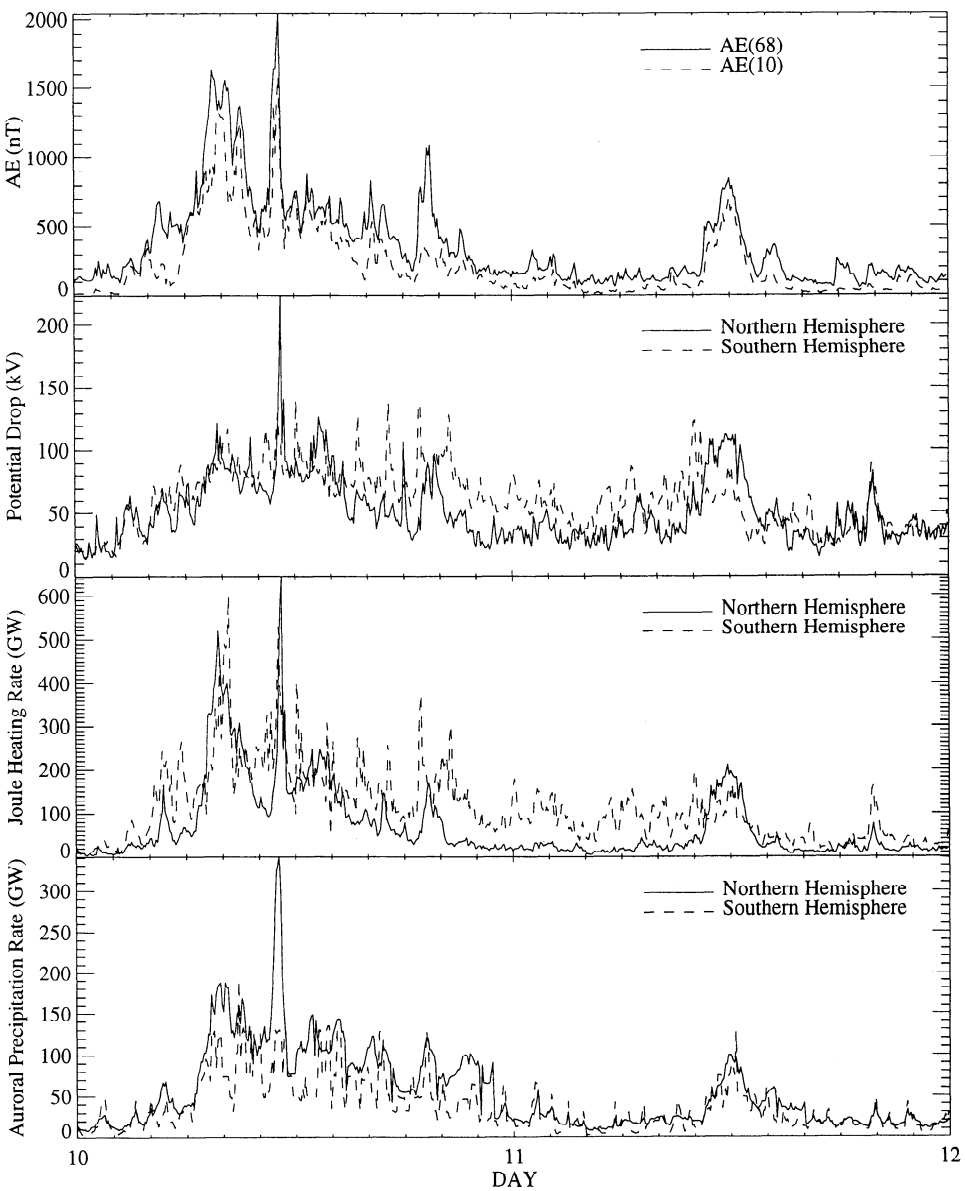

Figure 2. Distributions of various ionospheric quantities for the period of January 10–11, 1997.

satellites, auroral UVI images from the Polar satellite, ion drift measurements from 6 SuperDARN high frequency (HF) radars (all in the northern hemisphere) and from the Millstone Hill and Sondrestrom incoherent scatter (IS) radars, and magnetic perturbations monitored by 119 ground magnetometers distributed worldwide (among them 11 stations are located in the south polar region). Note that the Polar UVI images are available only during the northern hemisphere apogee passes from 1030 to 2300 UT on January 10 and from 0600 to 1600 UT on January 11. The Polar UVI images provide valuable information regarding the auroral precipitation of energetic electrons and ionospheric conductivity [*Lummerzheim et al.*, 1997; *Germany et al.*, 1997]. The 5-min snapshots of ionospheric conductance, auroral electron energy flux, electric potential, and Joule heating are derived by combining the various observations using the AMIE procedure.

2.3. High-Latitude Ionospheric Energy Deposition

Figure 2 shows the variations of the different parameters representing electrodynamic conditions at high latitudes over the period of January 10–11, 1997. The top panel shows the $AE(68)$ index (the solid curve), which is calculated from the north-south component of the magnetic perturbations measured by 68 ground stations located between 55° and 76° magnetic latitudes north and south. For comparison, the dashed curve is the AE index derived from 10 out of the 12 standard AE stations that are currently available for this study. The "standard" AE monitors reasonably well the general substorm activity during this period; but compared with $AE(68)$, it generally gives an underestimate of the activity, and sometimes misses substantially the auroral electrojets (for instance, at about 1900 UT on January 10). Over the 2-day period, the average value of $AE(10)$ is about 35% smaller than $AE(68)$.

The second panel presents the distribution of the cross-polar-cap potential drops in the northern and southern hemispheres. Potential drops of ~100 kV are reached when the IMF is southward. When the IMF points strongly northward, potential drops are in the order of 20–30 kV, a residual potential drop often ascribed to the "viscously driven" part of the solar wind-magnetosphere interaction [*Reiff and Luhmann*, 1986; *Knipp et al.*, 1993; *Lu et al.*, 1994]. The highest potential drop goes up to 220 kV, corresponding to the strongest AE burst (~2000 nT) during this period. The potential drops in the two hemispheres are roughly comparable. It is interesting to note that no apparent auroral activity is induced by the dramatic solar wind pressure enhancement at the rear of the cloud at early UT on January 11 (see Figure 1).

The bottom two panels show the hemisphere-integrated Joule heating rate U_J and auroral precipitation rate U_A above |50°| magnetic latitude, respectively. U_A is about the same as U_J during relatively quiet intervals, but is about one half of U_J during active intervals. The hemisphere-integrated Joule heating rate goes up to about 650 GW, whereas the peak value of U_A is about 340 GW. Note that the Joule heating rate calculated here does not take into account the neutral wind, which tends to reduce the total Joule heating by approximately 30% [*Lu et al.*, 1995].

Although we have gathered one of the most comprehensive data sets yet assembled, the data coverage in the southern hemisphere for this period is still relatively poor, with only 11 ground magnetometers and 5 satellites which all have an orbital period of ~110 min. The two HF radars in the southern hemisphere were either not in operation (Syowa) or of poor quality (Halley Bay). Consequently, the southern hemispheric results presented in Figure 2 are less reliable than those in the northern hemisphere. The 110-min modulations in the southern hemispheric potential drop and Joule heating shown in Figure 2 correspond to the intervals of DMSP overflights, similar to those reported by *Lu et al.* [1996].

2.4. Ring Current Energy Injection

In addition to the energy dissipated into the high-latitude ionosphere through Joule heating and auroral precipitation, energy that has been stored in the magnetosphere is partly converted into ring current energization that leads to the geomagnetic storm. A sophisticated calculation of the ring current energy injection requires detailed information about the dynamic properties of the inner magnetosphere. Unfortunately, information such as is not available for this particular period. We therefore invoke the empirical formula of *Akasofu* [1981] to estimate the ring current energy injection rate U_R:

$$U_R(GW) = -4 \times 10^4 \left(\frac{\partial Dst}{\partial t} + \frac{Dst}{\tau} \right) \qquad (1)$$

where τ in seconds is the ring current particle lifetime. For this study, we have chosen $\tau = 4$ hours for $Dst < -50$ nT, $\tau = 8$ hours for -50 nT $< Dst < -30$ nT, and $\tau = 20$ hours for $Dst > -30$ nT. Though the choice for τ is somewhat arbitrary, it is close to the values given by *Prigancova and Feldstein* [1992] in their model IV. The influence of the different τ values on the ring current energy injection rate is discussed in the next section.

The top panel of Figure 3 shows the different Dst values. The dashed curve is the standard Dst from 4 equatorial stations, the solid curve is the measured Dst from 18 stations, and the dotted curve is the pressure-corrected Dst [*Zwickl et al.*, 1987]. As one can see, the positive excursions are diminished in the pressure-corrected Dst, indicating that they are mainly due to the magnetopause current enhancement associated with the solar wind pressure impulses. The bottom panel shows the estimated ring current injection rate. The solid curve corresponds to the standard Dst, and the

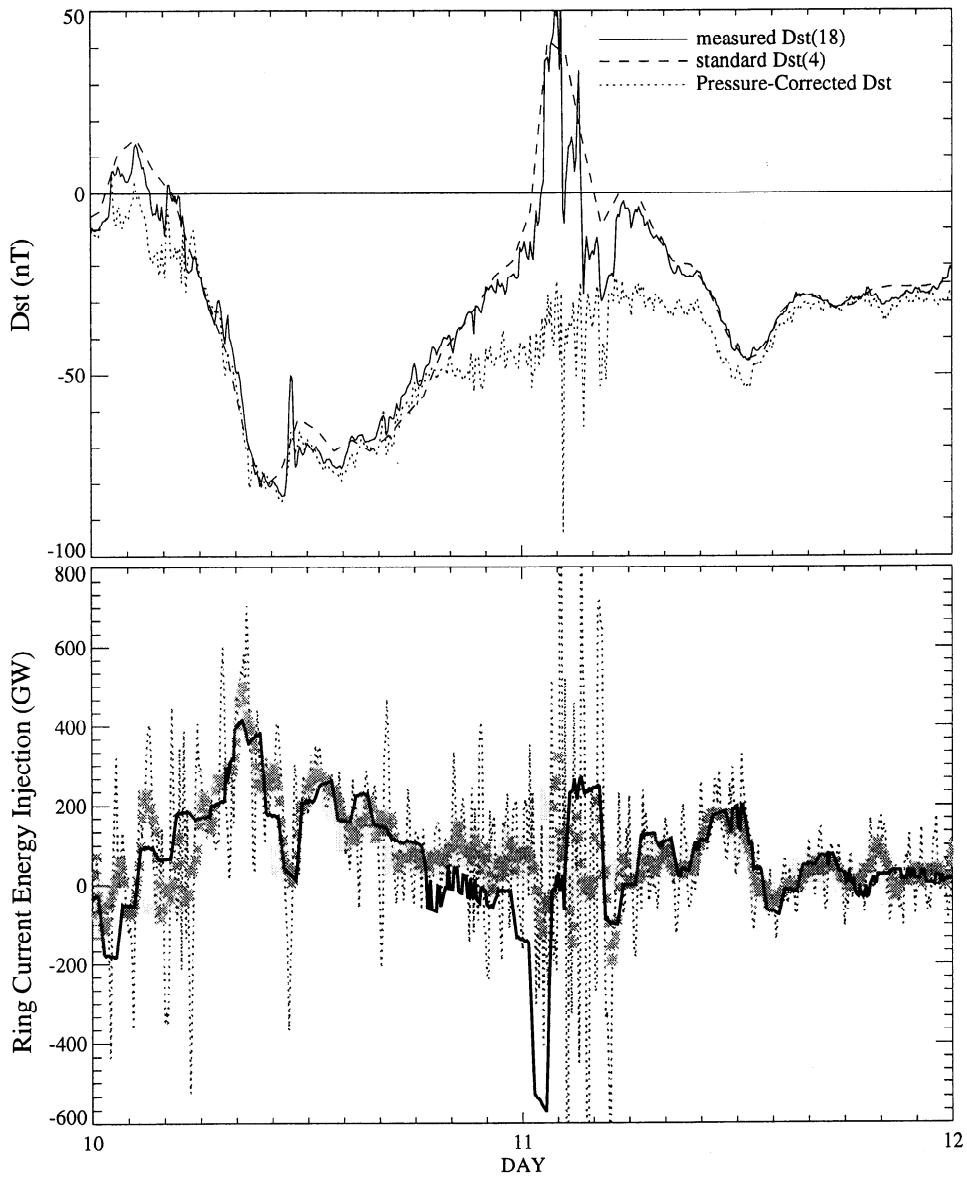

Figure 3. (top) The different *Dst* values. (bottom) The estimated ring current energy injections using the standard *Dst* (solid curve) and pressure-corrected *Dst* (dotted curve), respectively.

dotted curve uses the pressure corrected *Dst*. The dotted curve has many high-frequency fluctuations, and the thick shaded line is the 10-point running average which agrees reasonably well with the solid curve, except in the region of the large positive excursion associated with the strong solar wind pressure impulse at the trailing edge of the magnetic cloud. Compared with the ionospheric energy deposition shown in Figure 2, the peak value of the ring current energy injection is about two thirds of that due to Joule heating without neutral winds.

2.5. Solar Wind Energy Input

The solar wind is the ultimate energy source which is responsible for virtually all electrodynamic processes in the magnetosphere. The top panel of Figure 4 shows the solar wind kinetic power $U_{SW} = 1/2\rho V^3 A$, where ρ is the solar wind mass density, V is the solar wind radial speed, and A is the magnetopause cross section which depends on the solar wind dynamic pressure [*Shue et al.*, 1997]. The bottom panel shows the comparison of the solar wind electromagnetic energy transfer rate ($\epsilon = VB^2\sin^4(\theta/2)l_0^2$, where B is the IMF strength, θ is the angle between the z direction and the projection of the IMF in the y-z plane in GSM coordinates, and $l_0 = 7R_E$) [*Perreault and Akasofu*, 1978]) with the ionospheric energy deposition rate U_I (e.g., the sum of auroral precipitation and Joule heating rate integrated over both hemispheres) as well as the total magnetospheric energy deposition rate $U_T = U_I + U_R$. In general, there is a good correlation between ϵ and U_T. However, U_T is smaller than ϵ during the storm, and slightly larger be-

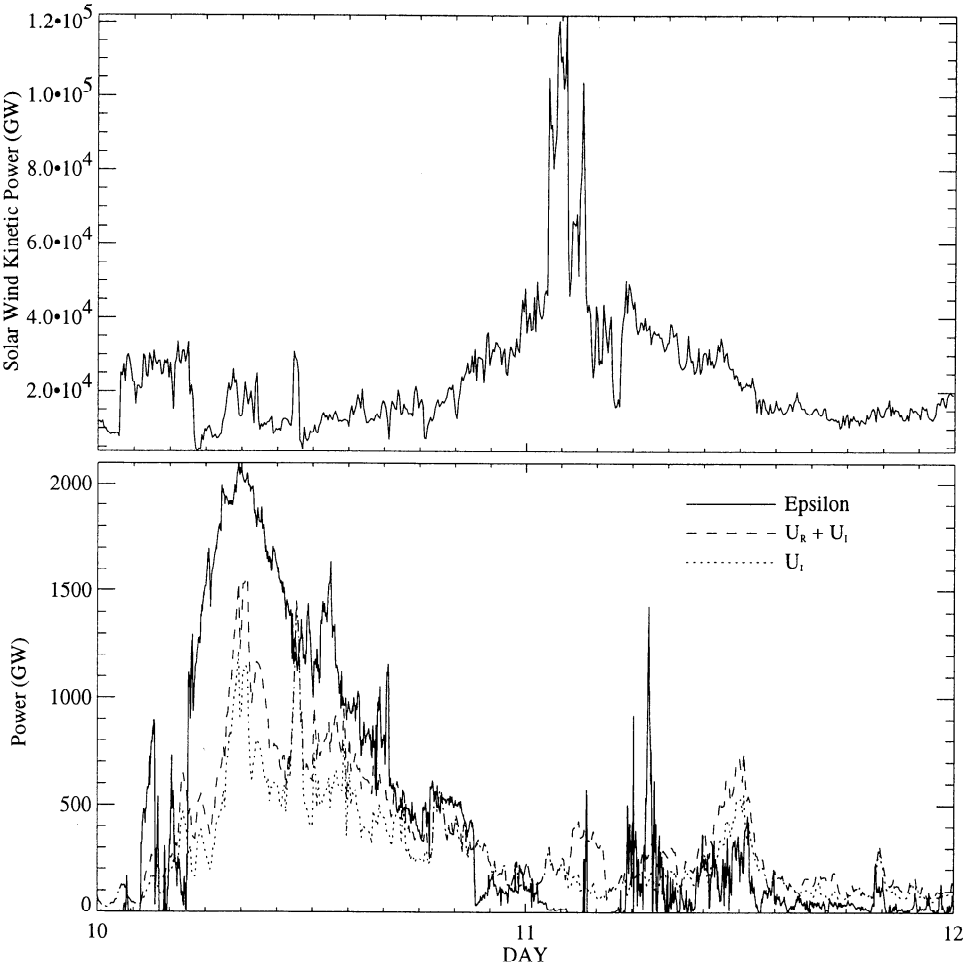

Figure 4. (top) Solar wind kinetic power. (bottom) Comparison of the solar wind electromagnetic power ϵ (solid line) to the total magnetospheric energy deposition rate U_T (dashed line) as well as the total ionospheric energy deposition rate U_I (dotted line).

fore and after the cloud. Note that after the passage of the magnetic cloud, the ϵ value become very small, but there is still sustained auroral activity that accounts for ~200 GW of power. Although the energy source during the quiet period may be due to the "unloading" process, it may also be attributed to the solar wind kinetic energy input through viscous interaction. As shown in the top panel of Figure 4, the available solar wind kinetic power is about 2 orders greater than the solar wind electromagnetic power (the ϵ parameter). However, it has little similarity with the profile of the magnetospheric energy deposition, implying that the solar wind kinetic energy input does not directly drive the magnetospheric electrodynamic processes. The overall coupling efficiency of the solar wind kinetic power to the magnetosphere is about 4%. However, the efficiency is much less, for example, during the passage of the high-density plug at around 0200 UT on January 11 (Figure 1). In this case, the magnetic field is northward so that the diminished efficiency reflects the fact that the overall effectiveness of the solar wind-magnetosphere coupling is reduced to the point where only the viscous interaction is left.

3. Discussion

As illustrated in Figure 2, during the 2-day period of January 10–11, 1997, the cross-polar-cap potential drop, Joule heating rate, and auroral precipitation seem well correlated with *AE*. A linear regression analysis is carried out to investigate this. Figure 5 shows the scatterplots of the different quantities in the northern (left) and southern (right) hemispheres versus *AE*(68). The linear correlation coefficient and the linear fitting of each quantity to *AE*(68) are given in each panel. The correlation coefficient r varies from 0.59 to 0.91 and is lower in the southern hemisphere than in the northern hemisphere. This is probably due to the fact that there are only three stations from the southern hemisphere that contribute to *AE*(68). Therefore the *AE*(68) index reflects mainly the auroral activity in the northern hemisphere. Additionally, the data coverage in the southern hemisphere is poorer than that in the northern hemisphere. From the linear fit, we find that the proportionality factor between Φ and *AE*(68) is 0.06 kV/nT in the northern hemisphere and 0.04 kV/nT in the southern hemisphere; the proportionality factor

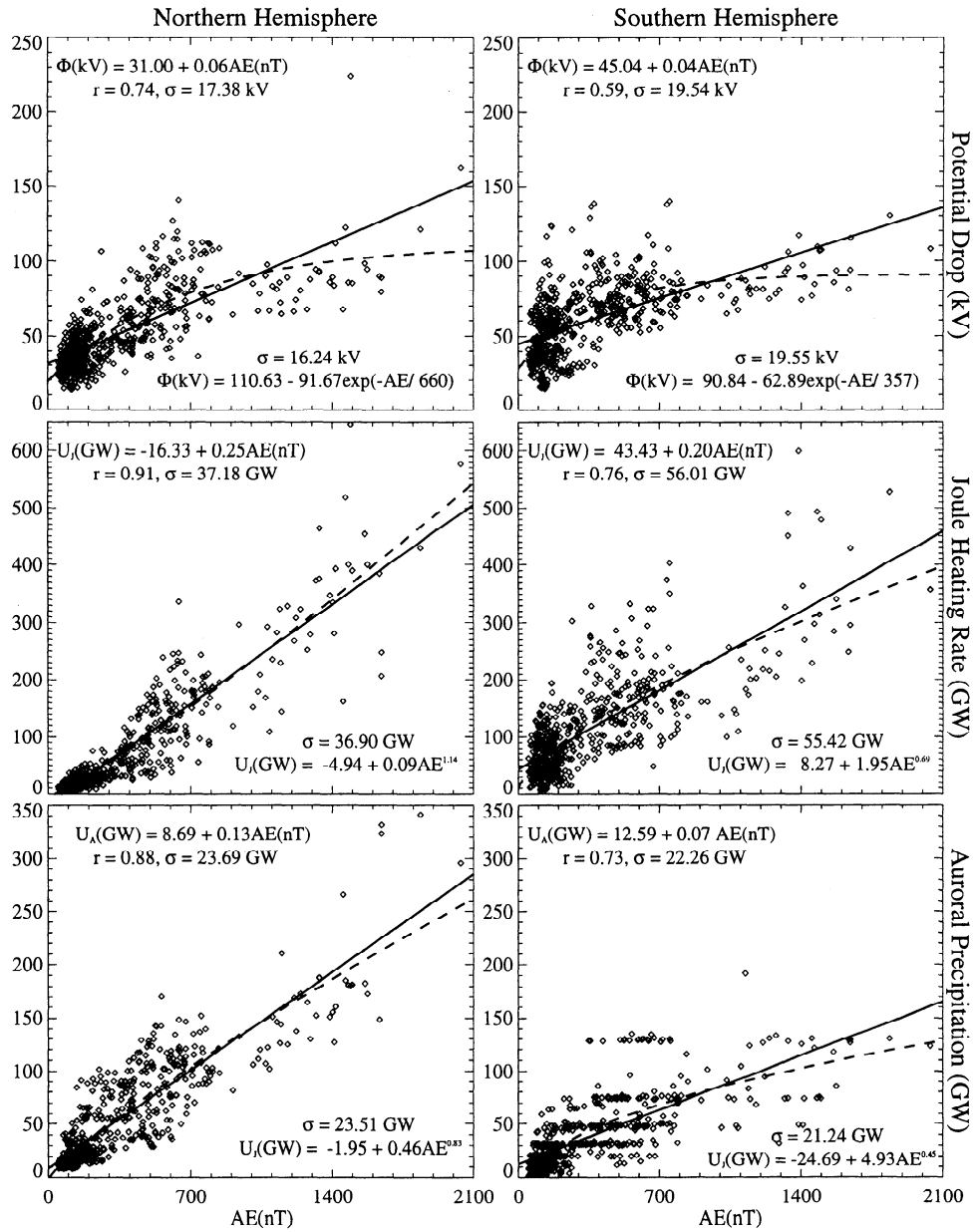

Figure 5. (from top to bottom) Scatterplots of the cross-polar-cap potential drop, hemisphere-integrated Joule heating rate, and hemisphere-integrated auroral precipitation versus *AE*. The left column is for the northern hemisphere, and the right column is for the southern hemisphere. The solid lines are linear fitting to the data, whereas the dashed lines are the nonlinear fitting. The r value represents the linear correlation coefficient, and σ is the standard deviation.

between U_J and $AE(68)$ is 0.25 GW/nT in the northern hemisphere and 0.20 GW/nT in the southern hemisphere; and the proportionality factor between U_A and $AE(68)$ is 0.13 GW/nT in the northern hemisphere and 0.07 GW/nT in the southern hemisphere. Previous studies have yielded different results from regression analyses for the different events, with a proportionality factor of Φ versus AE varying from 0.07 to 0.15 kV/nT, and a proportionality factor of U_J versus AE varying from 0.21 to 0.54 GW/nT [e.g., *Reiff et al.*, 1981; *Ahn et al.*, 1983, 1992; *Baumjohann and Kamide*, 1984; *Richmond et al.*, 1990; *Weimer et al.*, 1990; *Cooper et al.*, 1995]. Compared with previous studies, our results are close to the lower end of these values. The discrepancy among these independent studies may be attributed to several causes. First, a different AE index is used in the different studies. For instance, $AE(12)$ was used by Reiff et al., Richmond et al., and Weimer et al., but a multistation-derived AE was used in the rest of the studies as well as in this paper. Second, Φ and U_J are calculated using different methods. The study of Reiff et al. was statistically based; Ahn et al. and Baumjohann and Kamide used the Kamide-Richmond-Matsushita algorithm [*Kamide et al.*, 1981]; Richmond et al., Cooper et al., and this study apply the AMIE procedure. Finally, different seasons are involved in the

different studies. Seasonal variations can have a direct effect on the ionospheric conductivity, which in turn affect Joule heating. Because of the diversity of the different studies, caution should be taken when choosing empirical formulas to estimate ionospheric energy deposition.

Although the scatterplot of Figure 5 shows an overall linear correlation between AE and the various electrodynamic quantities, it is worthwhile testing if nonlinear functions would give a better fit to the data. The dashed lines in Figure 5 show the nonlinear least squares fitting to the data. As shown in the top panels, the cross-polar-cap potential drop tends to saturate after AE exceeds about 1000 nT; however, there are less than 10% data points (38 out of 576) with AE greater than 1000 nT. In the northern hemisphere, the inverse exponential fitting (i.e., Φ = a + b exp (-AE/c)) is slightly better than the linear fitting by reducing the standard deviation σ from 17.38 to 16.24 kV; but in the southern hemisphere, the nonlinear fitting yields a similar standard deviation as the linear fitting. *Weimer et al.* [1990] also performed both linear and nonlinear fits of AE versus Φ and found no significant difference between them. However, in their study there were only a couple of data points with AE >1000 nT. Whether the apparent asymptotic behavior of Φ with increasing AE is a real physical effect is certainly worth pursuing in future studies, and more date points with large AE values are desirable. Power function fits of AE versus U_J and U_A do not show any significant improvement over the linear fitting in terms of reducing the standard deviation.

It should be pointed out that we have taken into account the error δe associated with the estimated large-scale electric field E at each grid point when calculating the height-integrated Joule heating rate Q_J, e.g., $Q_J = \Sigma_P E^2 + \Sigma_P \langle(\delta e)^2\rangle$. Here the second term represents the adjustment to the Joule heating rate due to the variability in large-scale electric fields. As shown by *Lu et al.* [1996], although the general distribution is about the same, the magnitude of total hemisphere-integrated Joule heating rate U_J would be about 10–20% smaller without the second term. The AMIE-estimated Joule heating currently takes into account only the variability in large-scale (~150 km or greater) electric fields; however, it does not account for the variability in smaller-scale fields or in conductivities. Though the conductivity variability will alter the local distribution of Joule heating, it is unlikely to affect the total hemisphere-integrated Joule heating significantly because of cancellations between localized enhancements and reductions in conductivity. To what extent the smaller-scale field variations affect Joule heating is yet to be quantified, though theoretical calculations indicate that the small-scale E field fluctuations could increase Joule heating rate by about 30% [*Codrescu et al.*, 1995].

The magnitude of the ring current energy injection rate depends strongly on τ. The τ values chosen for this study seem to be reasonable because of the overall balance between the input solar wind energy and the total magnetospheric energy consumption (of course, this is only true if the ϵ parameter is indeed a good representation of the solar wind electromagnetic power). If we had used the τ value as suggested by *Zwickl et al.* [1987] (e.g., τ = 0.5 hour for ϵ >1000 GW), U_T would be 40% larger than ϵ during the storm. Recently, *Gonzalez et al.* [1994] have argued that the decay time τ should not be shorter than 1 hour, unless the storm is very intense. *Baker et al.* [1997] give a conservative estimate of the ring current injection rate using τ = 6 hours for their storm study. That storm had a minimum *Dst* of ~ -81 nT, which is close to the minimum *Dst* (-85 nT) of this study. By using the different τ values, the average ring current injection rate U_R over the main storm period of January 10–11 would become 266 GW (for τ = 1 hour), 124 GW (for τ = 4 hours), or 109 GW (for τ = 6 hours), respectively.

At present, the ϵ parameter of *Perreault and Akasofu* [1978] is widely used as a measure of the solar wind electromagnetic energy input to the magnetosphere. Since the justification of the ϵ function by *Akasofu* [1981] was based on the comparison of ϵ with the total magnetospheric energy consumption estimated from empirical formulas, it is expected that the solar wind energy input represented by ϵ will have some uncertainty. A quantification of this uncertainty has so far not been done. Furthermore, *Akasofu* [1981] argued that the effective cross-sectional area l_0^2 in the ϵ function should not strongly depend on solar wind conditions. However, the magnetopause model of *Shue et al.* [1997] indicates that the radius of the dawn-dusk magnetopause cross section changes from about 14 to 10 R_E during the passage of the magnetic cloud.

In our estimate of the magnetospheric energy budget, we have not included the energy that goes into precipitation of very energetic particles (>1 MeV) from the radiation belt and to plasma sheet heating, nor that which is associated with plasmoid ejections in the magnetotail and with tail lobe reconfiguration. For this particular period, the estimated energy flux of the MeV electrons measured by the SAMPEX satellite is about 0.5 GW, which is less than 1% of the total ionospheric energy deposition rate. It is difficult to estimate the energy deposition due to the plasma sheet heating, but a magnitude of 10^2 GW has been suggested by *Weiss et al.* [1992] as representative. Though plasmoid ejection can be a significant energy loss, it does not contribute to the net magnetospheric energy deposition since energy associated with plasmoids is originally extracted from and ultimately given back to the solar wind. Similarly, there is no net gain or loss in magnetic energy due to the magnetospheric reconfiguration throughout the

storm because the magnetosphere eventually resumes its original shape.

4. Summary

We have examined in this paper the global magnetospheric energy deposition during the January 1997 magnetic cloud event in terms of auroral precipitation and Joule heating in the high-latitude ionosphere as well as of ring current energy injection in the inner magnetosphere. During the 2-day storm period of January 10–11, the average globally integrated (summed over both hemispheres) Joule heating rate is 190 GW, the average ring current injection contributes 120 GW, and the average globally integrated auroral precipitation is 90 GW, resulting in a total magnetospheric energy deposition rate U_T of 400 GW. As a comparison, the average solar wind electromagnetic power (or the ϵ parameter) for the same 2-day period is 460 GW, and the solar wind kinetic power U_{SW} is 11,000 GW. However, the accuracy of the different energy budgets estimated in this study is subject to the availability of observations and the adequacy of knowledge in understanding the solar wind-magnetosphere coupling processes.

Variations of global ionospheric quantities, such as the cross-polar-cap potential drop, hemisphere-integrated Joule heating rate, and hemisphere-integrated auroral precipitation, represent important electrodynamic features associated with geomagnetic activity. A reasonably good correlation has been found between AE and the various ionospheric quantities, with a coefficient between 0.59 and 0.91. In the northern hemisphere where the data coverage is relatively good, a proportionality factor of 0.06 kV/nT is found for the potential drop versus AE, 0.25 GW/nT for Joule heating versus AE, and 0.13 GW/nT for auroral precipitation versus AE. Note that in this study, the AE index is based on observations from 68 ground magnetometers located between 55° and 76° magnetic latitude north and south. On average, the AE index thus obtained (i.e., $AE(68)$) is about 35% larger than the standard AE index. An apparent saturation of potential drop corresponding to large AE is found. However, more data points with AE >1000 nT are needed in order to verify if such asymptotic behavior is a profound feature of ionospheric electrodynamics.

Acknowledgments. The DMSP ion drift data were provided by M. Hairston at University of Texas at Dallas. The Kapuskasing HF radar is funded by NASA under grant NAG5-1099. The Goose Bay HF radar is supported by NSF under grant ATM-9502993. The Saskatoon HF radar is funded by an NSERC Canada Collaborative Special Project Grant. Millstone Hill radar operations are supported by NSF. CANOPUS magnetometer data was provided by the Canadian Space Agency. IMAGE magnetometer data used in this paper were collected as a German-Finnish-Norwegian-Polish project conducted by the Finnish Meteorological Institute. Data from U.S. Antarctic sites were provided by A. T. Weatherwax of the University of Maryland under NSF grant OPP9505823. Magnetometer data from Antarctic Syowa Station were provided from National Institute of Polar Research in Japan. Casey and Davis magnetometer data were supplied by Atmospheric and Space Physics group, Australian Antarctic Division. We wish to thank L. D. Morris for his efforts in collecting worldwide magnetometer data and making them available to this study via the on-line Space Physics Interactive Data Resource (SPIDR) operated by National Geophysical Data Center of NOAA, K. Yumoto and the STEL at Nagoya University for providing the 210 MM magnetic data, G. van Beek of the Geological Survey of Canada for providing the Canadian Geomagnetic Observatory data, M. Pinnock at the British Antarctic Survey for supplying the Halley magnetometer data, V. Papitashvili at University of Michigan for providing the Vostok magnetometer data, A. S. Potapov and S. I. Nechaev at the Institute of Solar-Terrestrial Physics at Irkutsk Observatory for providing the Irkutsk, Borok, Yukutsk, Tixie Bay, and Petropavlovsk data in Russia, and J. Posch for providing data from the MACCS stations. The MACCS project was supported by NSF grant ATM-9610072 to Augsburg College and ATM-9704766 to Boston University. Our acknowledgment also goes to C. Maclennan at Bell Laboratories, Lucent Technologies for the magnetometer data used in this study and to the Office of Polar Programs, National Science Foundation for support of the upper atmosphere physics program at McMurdo and South Pole. Work at HAO/NCAR was supported by the NSF Space Weather program. Work at UNH was supported in part by NASA grant NAG 5-2834 and by DARA grant 50 OC 8911 0. Work at PL was supported by AFOSR Task 2311G504. DL was supported by NASA grant NAG5-1097.

The Editor thanks John Foster for his assistance in evaluating this manuscript.

References

Ahn, B.-H., S.-I. Akasofu, and Y. Kamide, The Joule heating production rate and the particle energy injection rate as a function of the geomagnetic indices of AE and AL, *J. Geophys. Res., 88*, 6275, 1983.

Ahn, B.-H., Y. Kamide, H. W. Kroehl, and D. J. Gorney, Cross-polar cap potential difference, auroral electrojet indices, and solar wind parameters, *J. Geophys. Res., 97*, 1345, 1992.

Akasofu, S.-I., Energy coupling between the solar wind and the magnetosphere, *Space Sci. Rev., 28*, 121, 1981.

Baker, D. N., T. I. Pulkkinen, M. Hesse, and R. L. McPherron, A quantitative assessment of energy storage and release in the Earth's magnetosphere, *J. Geophys. Res., 102*, 7159, 1997.

Baumjohann, W., and Y. Kamide, Hemispherical Joule heating and the AE indices, *J. Geophys. Res., 89*, 383, 1984.

Burlaga, L. F., et al., A magnetic cloud containing prominence material: January 1997, *J. Geophys. Res., 103*, 277, 1998.

Codrescu, M. V., T. J. Fuller-Rowell, and J. C. Foster, On the importance of E-field variability for Joule heating in the high-latitude thermosphere, *Geophys. Res. Lett., 22*, 2393, 1995.

Cooper, M. L., C. R. Clauer, B. A. Emery, A. D. Richmond, and J. D. Winningham, A storm time assimilative mapping of ionospheric electrodynamics analysis for the severe

geomagnetic storm of November 8–9, 1991, *J. Geophys. Res., 100*, 19,329, 1995.

Farrugia, C. J., et al., Geoeffectiveness of three Wind magnetic clouds: A comparative study, *J. Geophys. Res.*, in press, 1998.

Farrugia, C. J., L. F. Burlaga, and R. P. Lepping, Magnetic clouds and the quiet/storm effect at Earth: A review, in *Magnetic Storms, Geophys. Monogr. Ser.*, vol. 98, edited by B. T. Tsururani et al., p. 91, AGU, Washington, D. C., 1997.

Fuller-Rowell, T. J., and D. S. Evans, Height-integrated Pedersen and Hall conductivity patterns inferred from the TIROS-NOAA satellite data, *J. Geophys. Res., 91*, 2242, 1986.

Germany, G. A., et al., Remote determination of auroral energy characteristics during substorm activity, *Geophys. Res. Lett., 24*, 995, 1997.

Gonzalez, W. D., J. A. Joselyn, Y. Kamide, H. W. Kroehl, G. Rostoker, B. T. Tsurutani, and V. M. Vasyliunas, What is geomagnetic storm? *J. Geophys. Res., 99*, 5771, 1994.

Kamide, Y., A. D. Richmond, and S. Matsushita, Estimation of ionospheric electric fields, ionospheric currents, and field-aligned currents from ground magnetic records, *J. Geophys. Res., 86*, 801, 1981.

Knipp, D. J., et al., Ionospheric convection response to slow, strong variations in a northward interplanetary magnetic field: A case study for January 14, 1988, *J. Geophys. Res., 98*, 19,273, 1993.

Lu, G., A. D. Richmond, B. A. Emery, and R. G. Roble, Magnetosphere-ionosphere-thermosphere coupling: Effect of neutral winds on Joule heating and field-aligned current, *J. Geophys. Res., 100*, 19,643, 1995.

Lu, G., et al., Interhemispheric asymmetry of the high-latitude ionospheric convection pattern, *J. Geophys. Res., 99*, 6491, 1994.

Lu, G., et al., High-latitude ionospheric electrodynamics as determined by the assimilative mapping of ionospheric electrodynamics procedure for the conjunctive SUNDIAL/ATLAS 1/GEM period of March 28–29, 1992, *J. Geophys. Res., 101*, 26,697, 1996.

Lummerzheim, D., M. Brittnacher, D. Evans, G. A. Germany, G. K. Parks, M. H. Rees, and J. F. Spann, High time resolution study of the hemispheric power carried by energetic electrons into the ionosphere during the May 19/20, 1996 auroral activity, *Geophys. Res. Lett., 24*, 987, 1997.

Perreault, P., and S.-I. Akasoku, A study of geomagnetic storms, *Geophys. J. R. Astron. Soc., 54*, 547, 1978.

Prigancova, A., and Y. I. Feldstein, Magnetospheric storm dynamics in terms of energy output rate, *Planet. Space Sci., 40*, 581, 1992.

Reiff, P. H., R. W. Spiro, and T. W. Hill, Dependence of polar cap potential drop on interplanetary parameters, *J. Geophys. Res., 86*, 7639, 1981.

Reiff, P. H., and J. G. Luhmann, Solar wind control of the polar cap voltage, in *Solar Wind-Magnetosphere Coupling*, edited by Y. Kamide and J. A. Slavin, p. 452, Terra Sci., Tokyo, 1986.

Richmond, A. D., and Y. Kamide, Mapping electrodynamic features of the high-latitude ionosphere from localized observations: Technique, *J. Geophys. Res., 93*, 5741, 1988.

Richmond, A. D., et al., Global measures of ionospheric electrodynamic activity inferred from combined incoherent-scatter radar and ground magnetometer observations, *J. Geophys. Res., 95*, 1061, 1990.

Shue, J.-H, J. K. Chao, H. C. Fu, C. T. Russell, P. Song, K. K. Khurana, and H. J. Singer, A new functional form to study the solar wind control of the magnetopause size and shape, *J. Geophys. Res., 102*, 9497, 1997.

Tsurutani, B. T., and W. D. Gonzalez, The efficiency of "viscous interaction" between the solar wind and the magnetosphere during intense northward IMF events, *Geophys. Res. Lett., 22*, 663, 1995.

Weiss, L. A., P. H. Reiff, J. J. Moses, and B. D. Moore, Energy dissipation in substorms, *Eur. Space Agency Spec. Publ., ESA-SP-335*, 309, 1992.

Weimer, D. R., N. C. Maynard, W. J. Burke, and C. Liebrecht, Polar cap potentials and the auroral electrojet indices, *Planet. Space Sci., 38*, 1207, 1990.

Zwickl, R. D., L. F. Bargatze, D. N. Baker, C. R. Clauer, and R. L. McPherron, An evaluation of the total magnetospheric energy output parameter, U_T, in *Magnetotail Physics*, edited by A. T. Y. Lui, p. 155, Johns Hopkins Univ. Press, Baltimore, Md., 1987.

B. N. Baker and X. Li, Laboratory of Atmospheric and Space Physics, University of Colorado, Campus Box 590, Boulder, CO 80309.

M. Brittnacher, Department of Geophysics, University of Washington, Seattle, WA 98122.

D. S. Evans, Space Environment Laboratory, NOAA, 325 Broadway, Boulder, CO 80303.

C. J. Farrugia, Space Science Center, University of New Hampshire, Durham, NH 03824.

R. Greenwald and J. M. Ruohoniemi, Applied Physics Laboratory, Johns Hopkins University, Laurel, MD 20742.

K. Hayashi, Department of Earth and Planetary Physics, University of Tokyo, Tokyo, 113 Japan.

R. P. Lepping, NASA Goddard Space Flight Center, Greenbelt, MD 20771.

M. Lester, Department of Physics, University of Leicester, Leicester, England LE1 7RH.

G. Lu, High Altitude Observatory, NCAR, PO Box 3000, Boulder, CO 80307-3000. (e-mail: ganglu@ncar.ucar.edu)

D. Lummerzheim, Geophysical Institute, University of Alaska, Fairbanks, AK 99775-7320.

G. Makarov, Institute of Cosmophysical Research and Aeronomy, Yakutsk, Russia.

R. L. McPherron, IGPP, University of California, Los Angeles, 405 Hilgard Avenue, Los Angeles, CA 90024-1567.

D. Milling, Department of Physics, University of York, York, England Y01 5DD.

T. Moretto, Danish Meteorologial Institute, Copenhagen, Denmark.

V. Odintzov and Z. Zaitzev, IZMIRAN, Moscow Region, 14209 Troitsk, Russia.

F. J. Rich, Phillips Laboratory, Hanscom Air Force Base, MA 01731.

G. Sofko, Department of Physics and Engineering Physics, University of Saskatchewan, 116 Science Place, Saskatoon, Saskatchewan, Canada S7N 5E2.

J. Thayer, SRI International, 333 Ravenswood Avenue, Menlo Park, CA 94025.

O. Troshichev, Geophysics Department, Arctic and Antarctic Research Institute, Institute Bering Street, 38 St. Petersburg 199226, Russia.

J. Villain, LPCE, CNRS, 3 Avenue Recherche Scientifique, 45071, Orleans, France.

(Received February 23, 1998; accepted February 27, 1998.)